13th ewtec 2019 Proceedings of the 13th European Wave and Tidal Energy Conference 1-6 Sept 2019, Naples, Italy

Numerical simulation of a latching controlled heaving-buoy-type point absorber by using a 3D numerical wave tank

Sung-Jae Kim, and Weoncheol Koo

Abstract—**The aim of this study is to estimate the nonlinear effect of a heaving-buoy-type wave energy converter (WEC) under various environmental conditions such as nonlinearities due to high amplitude waves, sea bottom, power take-off (PTO) system and PTO control strategy. To consider those nonlinearities from WEC, a three-dimensional potential numerical wave tank technique (3D-PNWT) was adopted. The PNWT was based on the potential flow theory and the boundary element method (BEM). The mixed Eulerian and Lagrangian (MEL) method and the acceleration potential approach were applied to describe nonlinear wave behaviours and the wave-body interactions (WBI). In addition, the hydraulic PTO system was numerically modelled as an approximate coulomb damping force for reducing numerical errors. The latching control strategy for PTO operation was applied, which is one of the famous discrete phase control strategy.**

By applying the hydraulic PTO system with the latching control strategy in the 3D-PNWT, a parametric study was performed on wave steepness, water depth and the latching duration. Through this, various nonlinear effects on WEC performance were compared in detail.

Keywords—**3D potential numerical wave tank, Wave-body interaction, Nonlinear waves, Hydraulic power take-off system, Latching control strategy, Fully nonlinear**

I. Introduction

Numerous studies are underway to design for buoy-type wave energy converters (WEC). The frequency domain hydrodynamic analysis is usually performed based on linear body motion in the linear wave theory (Airy wave theory). However, the WEC produces generally much wave energy under high waves because the higher the wave height, the more energy has. Since the high wave causes wave nonlinearity, nonlinear wave has to be considered in the simulation. In addition, the effect of the sea bottom on the WEC performance near shore area should also be considered.

The potential Numerical Wave Tank (PNWT) can be a suitable analysis approach to simulate nonlinear waves, wave-sea bottom effect and wave-body interaction at once ([1]-[5]). It is based on the potential flow theory and the boundary element method (BEM). The mixed Eulerian and Lagrangian method (MEL) and the acceleration potential approach were adopted to simulate nonlinear waves and describe the wave-body interaction in the time domain. Some researchers carried out numerical studies by using a 2D-PNWT for a fixed or a floating Oscillating Water Column (OWC) type WEC ([6]-[9]). Kim ([10]) and Kim *et al.* ([11]) performed a hydrodynamic direct time domain analysis for a heaving-buoy-type point absorber using a 3D-PNWT. Kim ([10]) showed the basic validation for a 3D-PNWT and carried out the wave-body-Power-Take-off (PTO) interaction. Kim *et al.* ([11]) compared the difference of various calculation methods such as linear, partially nonlinear and fully nonlinear analysis based on the potential flow theory. The partially nonlinear analysis considers instantaneous nonlinear Froude-Krylov force acting on the body, although other forces are considered as linear terms from the frequency domain analysis ([12]-[15]). The fully nonlinear analysis is to simulate nonlinear wave generation, propagation and wave-body interaction at every time step, which is very similar to a physical wave tank experiment.

In this study, a 3D-PNWT was adopted to solve the interaction of wave-sea bottom and wave-body. The PNWT was based on the method of Kim ([10]). The MEL method and the acceleration potential approach were applied. The 2nd-order stokes' wave was generated as an input wave. For open sea condition, the artificial damping zone scheme was adopted at the end of boundary. The hydraulic PTO system was installed in the WEC and modelled numerically as an approximate coulomb damping force ([16]-[18]).

The latching control strategy was applied to the PTO system to amplify the extracted power from WEC. The latching control is a famous discrete phase control of buoy motion forcibly for a certain time. Therefore, to simulate the wave-buoy-PTO system with latching control in the time domain precisely, fully nonlinear analysis using a 3D-PNWT is required. The results of nonlinear calculation were compared with linear analysis.

ID number and the conference track : 1336 / WHM

S.J. Kim and W. Koo are with the Department of Naval Architecture and Ocean Engineering, INHA University, Incheon, Republic of Korea (1st author e-mail : sungjaekim1001@gmail.com, 2nd author e-mail : wckoo@inha.ac.kr)

 Copyright © European Tidal and Wave Energy Conference 2019

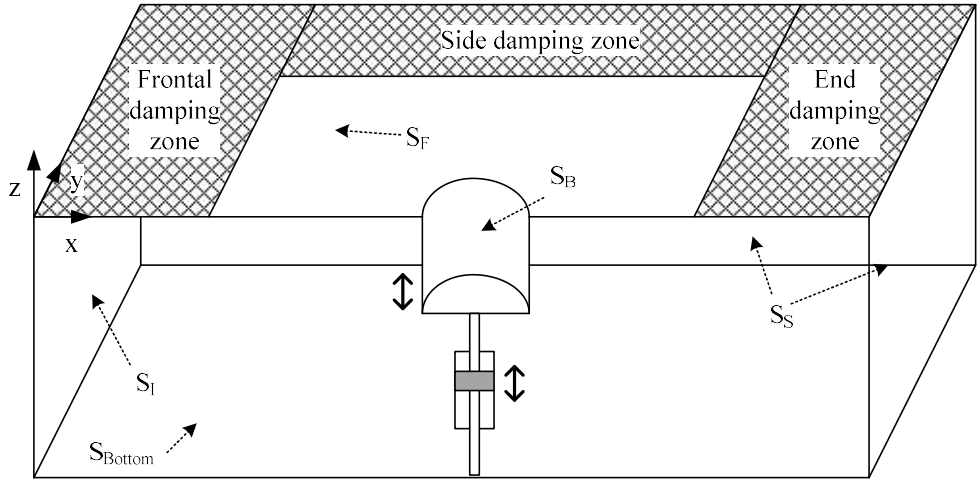

Fig. 1. Overview of a three-dimensional potential numerical wave tank for a heaving buoy type wave energy converter.

II. MATHEMATICAL FORMULAE

A. Potential Numerical Wave Tank

The 3D-PNWT is a suitable numerical technique to simulate nonlinear waves and wave-body interaction in the time domain. The computational domain includes a wave maker, free surfaces, a rigid buoy and rigid side wall and bottom, which conditions are very similar to a physical wave tank. The PNWT was based on the potential flow theory and BEM. So, the governing equation is the Laplace equation (1) and it can be transferred to the boundary integral equation by using the Green's 2nd identity.

$$\nabla^2\phi = 0 \tag{1}$$

$$\alpha\phi_i = \iint_\Omega \left(G_{ij}\frac{\partial\phi_j}{\partial n} - \phi_j\frac{\partial G_{ij}}{\partial n}\right) dS \ \text{ in } \Omega \tag{2}$$

where ϕ is the velocity potential. α and G_{ij} are the solid angle and the green function, respectively.

The kinematic boundary conditions for body boundary, incident wave boundary and side wall boundary can be expressed respectively as (3-5).

$$\frac{\partial\phi}{\partial n} = \vec{V}\cdot\vec{n} \ \text{ on } S_B \tag{3}$$

$$\begin{aligned}\frac{\partial\phi}{\partial n} &= n_x\frac{\partial\phi}{\partial x} \\ &= n_x\frac{gAk}{\omega}\frac{\cosh k(z+h)}{\cosh kh}\cos(kx-\omega t) \qquad \text{on } S_I \\ &+ n_x\frac{3}{4}A^2\omega k\frac{\cosh 2k(z+h)}{\sinh^4 kh}\cos 2(kx-\omega t)\end{aligned} \tag{4}$$

$$\frac{\partial\phi}{\partial n} = 0 \ \text{ on } S_S \tag{5}$$

where, $\vec{V}$ and $\vec{n}$ are velocity of the rigid body and normal vector. g, A, k, h and ω denote the gravitational acceleration, wave amplitude, wave number, water depth and wave frequency, respectively. S_B, S_I and S_S are the body surface, incident wave boundary surface and side-wall boundary surface, as shown in Fig. 1. To reduce the number of calculation nodes, the sea bottom boundary was expressed by the image method. The incident wave was generated by applying the wave profile of 2nd-order Stokes' waves. On the other hand, the linear wave was generated in linear analysis and partially nonlinear analysis.

The free surface boundary condition can be described as the dynamic boundary condition and kinematic boundary condition (6-7).

$$\frac{\partial\phi}{\partial n} = -g\eta - \frac{1}{2}\left|\nabla\phi\right|^2 + \nabla\phi\cdot\vec{v} \ \text{ on } S_F \tag{6}$$

$$\frac{\partial\eta}{\partial t} = \frac{\partial\phi}{\partial z} - \left(\nabla\phi - \vec{v}\right)\cdot\nabla\eta \ \text{ on } S_F \tag{7}$$

where, $\vec{v}$ is the nodal velocity on the surface. In this study, the semi-Lagrangian method was applied to describe the free surface calculation nodes. The nodal velocity can be described as $\vec{v} = \left(0, 0, \partial\eta/\partial t\right)$. To express open sea condition, the artificial damping scheme was adopted, the same shape of [19]. The length of artificial damping zone is set to one wave length.

The acceleration potential approach was also used to calculate the instantaneous exact total force acting on the body. The indirect method was additionally adopted to calculate the buoy displacement. Finally, the total force

can be expressed as (8) with the acceleration potential approach and indirect method.

$$F_i = \int_{S_B} -\rho\left(a_i\varphi_i + \varphi_7 + gz + \frac{1}{2}\left|\nabla\phi\right|^2 \right) dS - W\delta_{i3} \qquad (8)$$

where, φ is the acceleration potential. W is weight of a buoy. GMRES method for matrix calculation and Chebyshev five-point smoothing scheme were used. Details can be found in [10]. For time marching, the Runge-Kutta 4th-order method for time integration was applied.

B. PTO system

The hydraulic PTO system was adopted in the present simulation. It consists of the hydraulic cylinder, hydraulic motor and generator. The force acting on the body from the hydraulic PTO can be expressed as (9) ([18]).

$$F_{PTO} = -\min(Gx_i, sign(\Delta pS_c)) \qquad (9)$$

where, Δp and S_c are the difference between High Pressure (HP) and Low Pressure (LP) of the cylinder, and the sectional area of the cylinder, respectively. G is the slope of the PTO force to reduce numerical error. The error occurs due to an excessive PTO force from very small motion of the buoy. It is set to 10 times the coulomb damping force. In this study, the double-acting hydraulic cylinder was considered, which inner sectional areas of both sides are same.

C. Latching control strategy

Folley *et al*. [20] showed the phase control strategy for a heaving-buoy-type point absorber can maximize the extracted wave power. The latching control is one of the famous discrete phase control strategies. This control is that the buoy motion is constraint during a certain time, which is called 'latching duration', when the buoy displacement reaches its peak. In this control strategy, an optimal value of latching duration is a very important parameter.

The phase control can amplify the buoy displacement against incident waves and the extracted power increases in the hydrodynamic analysis. In this study, the fully nonlinear analysis was conducted by using a 3D-PNWT technique. The fully nonlinear analysis means that nonlinear effect of instantaneous total force acting on the body is simulated in the time domain. Total forces include the radiation, diffraction, nonlinear Froud-Kyrlov and restoring force. Comparing the RAOs of buoy and the extracted powers for various numerical methods such as linear, partially nonlinear and fully nonlinear analysis, nonlinear effect of all relevant parameters on WEC performance can be estimated.

III. NUMERICAL MODEL AND RESULTS

In this study, a cylindrical shaped buoy was considered. Its draft (d) and radius (R) are both 1.0 m. The weight of buoy (W) is 3.141 ton. The calculation domain is x-axis symmetric to reduce calculation nodes on the domain. Table 1 shows the specification of a buoy, a hydraulic cylinder and input wave conditions. The cylindrical buoy is located on the centre of computational domain. The dimension of domain is four wavelengths in the transverse direction and two wavelengths in the longitudinal direction. The input wave period was only considered as the heave natural period of buoy (3.0 sec). The number of elements per one wave length is 20. And the integration time step was set to T(Wave period)/50. Fig. 2 shows the snapshot of 3D-PNWT when simulation time is 6 and 10 times wave period, respectively. It is a clear feature of the 3D-PNWT that the incident wave is generated and proceeds to the buoy in the domain. The artificial damping zone was applied to the end of the free surface boundary to satisfy the open sea condition. As shown in fig. 2, the artificial damping zone is working well.

The latching control strategy was also applied to the PTO system in a heaving-buoy-type WEC. Firstly, various latching durations were applied to obtain an optimal value. Fig. 3 shows heave RAOs on various latching durations at the heave natural period (T = 3 sec) of the buoy. In this case, the deep water condition and linear wave condition (small amplitude wave) were considered. When the latching duration was 0.2 s, the maximum heave RAO occurred. The heave RAO was found to be doubled with an optimal latching duration, compared with no phase control (T_L = 0 s).

TABLE I
SPECIFICATION OF DIMENSIONS OF A BUOY AND THE HYDRAULIC PTO SYSTEM

Item	Unit	Dimension
Draft of a buoy	m	1.0
Radius of a buoy	m	1.0
Weight of a buoy	ton	3.141
H/λ		0.02~0.05
h/λ		0.2~0.5
F_{PTO}/F_Z		0.4
Latching duration	s	0.1~0.8

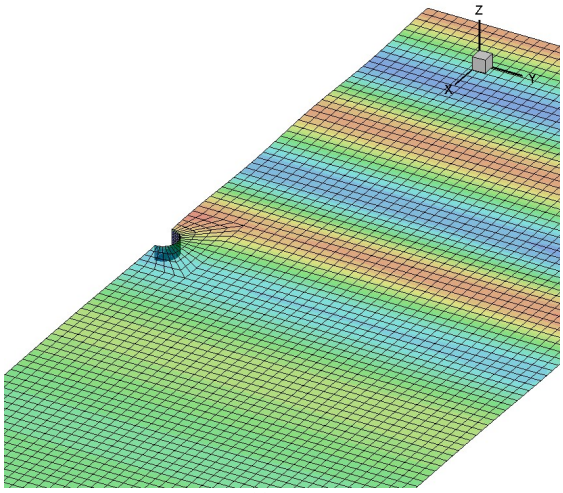

(a) t=6T

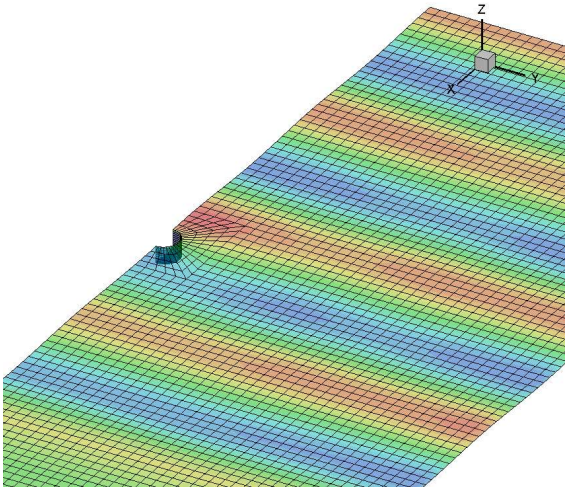

(b) t=10T

Fig. 2. Snapshot of a 3D potential numerical wave tank for a heaving-buoy-type wave energy converter (T = 3 s, H/λ = 1/50, h/λ = 1/2, F_{PTO}/F_Z = 0.4).

TABLE II
DIFFERENCE OF CALCULATION PROCEDURE BETWEEN LINEAR, PARTIALLY NONLINEAR AND FULLY NONLINEAR ANALYSIS

	Linear analysis	Partially nonlinear analysis	Fully nonlinear analysis
Incident waves	Linear	Linear	Stokes 2nd wave
Nonlinear waves	X	X	O
Nonlinear buoy motion	X	O	O

The optimal latching duration (0.2 s) was then applied to all calculation cases of this study. The hydrodynamic and PTO performance of WEC were estimated under various water depths and wave steepness conditions. Fig. 4 shows heave RAOs and time-averaged extracted powers on various analysis methods and water depth conditions. In this case, small wave steepness condition was adopted (H/λ = 1/50). Optimal PTO force and latching

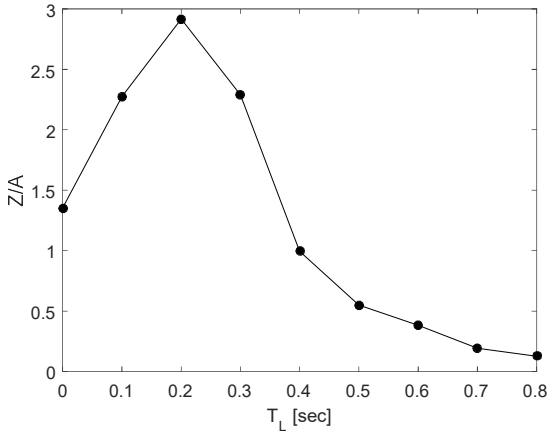

Fig. 3. Comparison of heave RAO on various latching duration (T = 3 s, H/λ = 1/50, h/λ = 1/2, F_{PTO}/F_Z = 0.4).

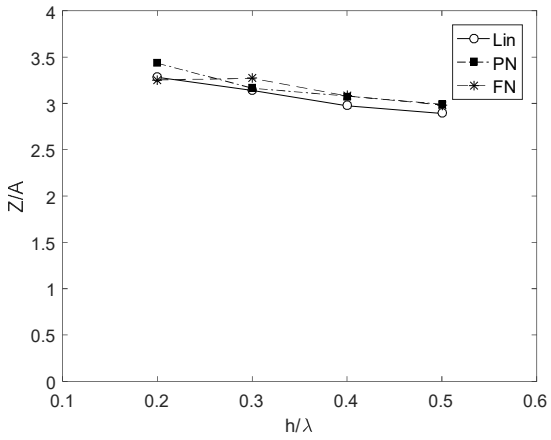

(a) Heave RAO

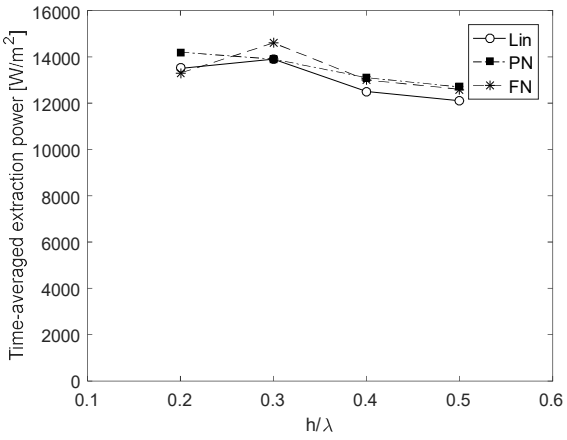

(b) Time-averaged extraction power

Fig. 4. Comparison of (a) heave RAO and (b) time-averaged extraction power on various water depth conditions.

(T = 3 s, H/λ = 1/50, F_{PTO}/F_Z = 0.4, T_L = 0.2 s, 'Lin' : Linear analysis, 'PN' : Partially nonlinear analysis, 'FN' : Fully nonlinear analysis)

duration were also used (F_{PTO}/F_z = 0.4, T_L = 0.2 s). Table 2 shows the difference of calculation procedure between the linear, partially nonlinear (PN) and fully nonlinear (FN) analysis in the time domain. The linear analysis included linear input waves with linear buoy motion. The

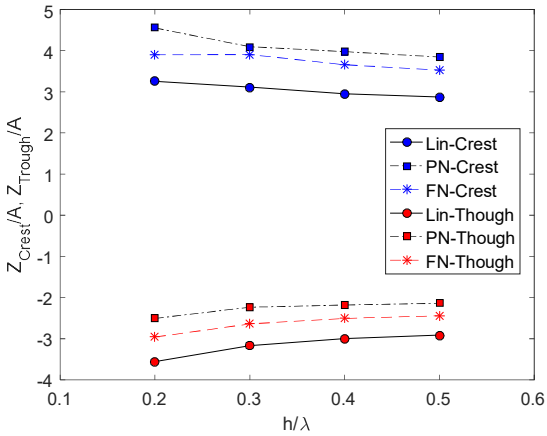

Fig. 5. Comparison of non-dimensional buoy motion crest and wave trough on various water depth conditions.

(T = 3 s, H/λ = 1/50, F_{PTO}/F_Z = 0.4, T_L = 0.2 s, 'Lin' : Linear analysis, 'PN' : Partially nonlinear analysis, 'FN' : Fully nonlinear analysis)

PN analysis considers nonlinearity of buoy motion by re-gridding the calculation nodes of a buoy according to buoy displacement. This is also based on linear waves without wave nonlinearity. On the other hand, the FN analysis can simulate both wave nonlinearity and the nonlinearity of buoy motion. This method can calculate and simulate wave-body interaction by rearranging all calculation nodes instantaneously according to wave elevation and buoy motion. In Fig. 4, the heave RAO decreases as water depth increases. The difference between linear and nonlinear results (PN and FN) was small (less than 5 %) according to water depth condition.

Fig. 5 shows the height of buoy motion crest and trough on various water depth conditions. The results of PN showed a large crest and small trough due to the relatively large buoy motion. This is caused by the effect of nonlinear Froude-Krylov force. The results of FN showed low crest and deep trough compared to those of PN, which may be a nonlinear wave effect.

Fig. 6 shows heave RAOs and extracted powers on various wave steepness conditions. Generally, wave nonlinearity increases as wave steepness increases. The difference between the linear analysis and nonlinear analysis (PN and FN) reached up to 30 % under high wave steepness (H/λ = 0.05, 1/20). However, the difference between both nonlinear results was small. Therefore, the difference between linear and nonlinear results is mainly due to body nonlinearity. Fig. 7 shows the crest and trough of buoy displacement on various wave steepness conditions. The body motion (crest to trough) in the nonlinear analysis (PN, FN) was formed above the mean water level. As wave steepness increases, the crest of body motion decreases and the trough of body motion increases due to the nonlinear buoy displacement. However, in the linear analysis, the average of body motion was located at mean water level regardless of wave steepness.

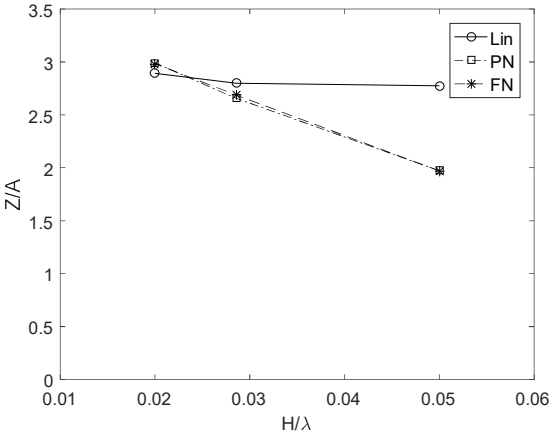

(a) Heave RAO

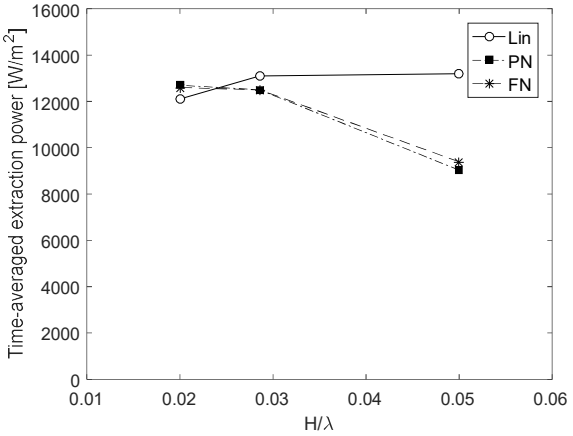

(b) Time-averaged extraction power

Fig. 6. Comparison of heave RAO (a) and the time-averaged extraction power (b) on various wave steepness conditions.

(T = 3 s, h/λ = 1/2, F_{PTO}/F_Z = 0.4, T_L = 0.2 s, 'Lin' : Linear analysis, 'PN' : Partially nonlinear analysis, 'FN' : Fully nonlinear analysis)

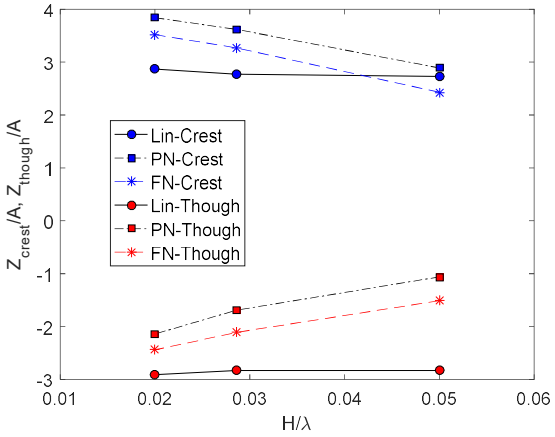

Fig. 7. Comparison of non-dimensional buoy motion crest and wave trough on various wave steepness conditions.

(T = 3 s, h/λ = 1/2, F_{PTO}/F_Z = 0.4, T_L = 0.2 s, 'Lin' : Linear analysis, 'PN' : Partially nonlinear analysis, 'FN' : Fully nonlinear analysis)

IV. CONCLUSION

In this study, numerical study on a latching controlled buoy-type WEC was conducted by using a three-

dimensional potential numerical tank to estimate nonlinear effect of hydrodynamic and PTO performance of WEC. The PNWT was based on the potential flow theory and BEM. The MEL method and the acceleration potential approach were used to simulate the nonlinear waves and wave-body interactions. The hydraulic PTO system was numerically modelled as an approximate coulomb damping force and applied to the 3D-PNWT. Additionally, the latching control strategy was also applied to PTO system to maximize the extracted wave power in WEC.

Optimal PTO force and latching duration were determined by comparing the results for various conditions, and then the optimal values were applied to the WEC in the 3D-PNWT. Three different hydrodynamic analyses such as linear, partially nonlinear and fully nonlinear analysis were performed and compared their results. The heave RAOs and time-averaged extracted powers were compared for various wave steepness and water depth conditions. The difference of RAOs between linear and nonlinear results (PN and FN) was small according to water depth condition.

The motion of buoy from nonlinear results showed a large crest and small trough due to the effect of nonlinear Froude-Krylov force. The motion was also formed above the mean water level. However, in the linear analysis, the average of body motion was located at mean water level, regardless of wave steepness.

The wave nonlinearity increased with an increase of wave steepness. The difference of heave RAOs and extracted powers between the linear and the nonlinear analysis reached up to 30 % under high wave steepness. This was mainly due to body nonlinearity.

ACKNOWLEDGEMENTS

This work was financially supported by the "Korea-UK Global Engineer Education Program for Offshore Plant" through the Ministry of Trade, Industry & Energy (MOTIE) and Korea Institute for Advancement of Technology (KIAT), Korea. This research was also supported by Basic Science Research Program through the National Research Foundation of Korea (NRF), funded by the Ministry of Science, ICT & Future Planning (NRF-2018R1A6A3A01013558).

REFERENCES

[1] T. Tanizawa, "A nonlinear simulation method of 3-D body motions in waves (1st Report)", Journal of the Society of Naval Architects of Japan, pp. 171-191, 1995.

[2] W. Koo and M.H. Kim, "Freely floating-body simulation by a 2D fully nonlinear numerical wave tank", Ocean Engineering, vol. 31, pp. 2011–2046, 2004.

[3] W. Bai and R. Eatock Taylor, "Fully nonlinear simulation of wave interaction with fixed and floating flared structures", Ocean Engineering, vol. 36, no. 3, pp. 223-236, 2009.

[4] L. Letournel, P. Ferrant, A. Babarit, G. Ducrozet, J.C. Harris, M. Benoit and E. Dombre, "Comparison of fully nonlinear and weakly nonlinear potential flow solvers for the study of wave energy converters undergoing large amplitude motions", In ASME 2014 Proceedings of the 33rd International Conference on Ocean, Offshore and Arctic Engineering, American Society of Mechanical Engineers, San Francisco, California, USA, 2014

[5] B.Z. Zhou, D.Z. Ning, B. Teng and W. Bai, "Numerical investigation of wave radiation by a vertical cylinder using a fully nonlinear HOBEM", Ocean Engineering, vol. 70, pp. 1–13, 2013.

[6] W. Koo and M.H. Kim, "Nonlinear Time-Domain Simulation of a Land-Based Oscillating Water Column", Journal of waterway, port, coastal and ocean engineering, vol.136, no. 5, pp. 276-285, 2010.

[7] D.Z. Ning, J. Shi, Q.P. Zou and B. Teng, "Investigation of hydrodynamic performance of an OWC(oscillating water column) wave energy device using a fully nonlinear HOBEM(higher-order boundary element method)", Energy, vol. 83, pp. 177-188, 2015.

[8] K.R. Lee, W. Koo and M.H. Kim, "Fully nonlinear time-domain simulation of a backward bent duct buoy floating wave energy converter using an acceleration potential method", International Journal of Naval Architecture and Ocean engineering, vol. 5, pp. 513–528, 2013.

[9] S.J. Kim, W. Koo and M.H. Kim, "Nonlinear time-domain NWT simulations for two types of a backward bent duct buoy (BBDB) compared with 2D wave-tank experiments", Ocean Engineering vol. 108, pp. 584–593, 2015.

[10] S.J. Kim, "Numerical study on a floating wave energy converter with a nonlinear PTO system", Ph.D. dissertation, Univ. of Ulsan, Republic of Korea, 2018 (In Korean)

[11] S.J. Kim, W. Koo and M.J. Shin, "Numerical study on nonlinear hydrodynamic performance of a heaving buoy type wave energy converter under nonlinear wave condition", *Advances in Renewable Energies Offshore : Proceedings of the 3rd international conference on Renewable Energies Offshore (RENEW 2018)*, Lisbon, Portugal, pp. 291-295, 2018.

[12] A. Babarit and A.H. Clement, "Declutching control of a wave energy converter". Ocean Engineering, vol. 36, pp.1015–24, 2009.

[13] A. Merigaud, J.C. Gilloteaux, and J.V. Ringwood, "A nonlinear extension for linear boundary element methods in wave energy device modelling", *in Proceedings of the ASME 2012 31st International Conference on Ocean, Offshore and Arctic Engineering OMAE2012*, Rio de Janeiro, Brazil, 2012.

[14] G. Giorgi and J.V. Ringwood, "Computationally efficient nonlinear froude-krylov force calculations for heaving axisymmetric wave energy point absorbers", Journal of Ocean Engineering and Marine Energy, vol. 3, pp. 21–33, 2017.

[15] G. Giorgi and J.V. Ringwood, "Analytical representation of nonlinear Froude-Krylov forces for 3-DoF point absorbing wave energy devicses", Ocean Engineering, vol. 164, pp. 749-759, 2018.

[16] A. Babarit, J. Hals, M.J. Muliawan, A. Kurniawan, T. Moan and J. Krokstad, "Numerical benchmarking study of a selection of wave energy converters", Renewable Energy, vol. 41, pp.44-63, 2012.

[17] A.F.O. Falcao, "Phase control trough load control of oscillating-body wave energy converters with hydraulic PTO system", Ocean engineering, vol. 35, pp. 358-366, 2018.

[18] S.J. Kim, W. Koo and M.J. Shin, "Numerical and experimental study on a hemispheric point-absorber-type wave energy converter with a hydraulic power take-off system", Renewable energy, vol. 135, pp. 1260-1269, 2019.

[19] M.W. Kim, W. Koo and S.A. Hong, "Numerical analysis of various artificial damping schemes in a three-dimensional numerical wave tank", Ocean Engineering, vol. 75, pp. 165-173, 2014.

[20] M. Folley, A. Henry and T. Whittaker, "Contrasting the hydrodynamics of heaving and surging wave energy converter,"

In: *Proceedings of the 11th European Wave and Tidal Energy conference*, Nantes, France, 2015.